Optics Letters

Two-photon Shack–Hartmann wavefront sensor

Fei Xia,*,† David Sinefeld,† Bo Li, and Chris Xu

School of Applied and Engineering Physics, Cornell University, Ithaca, New York 14853, USA
*Corresponding author: fx43@cornell.edu

Received 20 January 2017; accepted 10 February 2017; posted 21 February 2017 (Doc. ID 283968); published 10 March 2017

We introduce a simple wavefront sensing scheme for aberration measurement of pulsed laser beams in near-infrared wavelengths (<2200 nm), where detectors are not always available or are very expensive. The method is based on two-photon absorption in a silicon detector array for longer wavelengths detection. We demonstrate the simplicity of such implementations with a commercially available Shack–Hartmann wavefront sensor and discuss the detection sensitivity of this method.

OCIS codes: (190.0190) Nonlinear optics; (010.7350) Wave-front sensing; (140.3295) Laser beam characterization.

https://doi.org/10.1364/OL.42.001141

Wavefront sensing is an important tool in optical testing and is an essential part of beam characterization for both industrial and research applications. The ability to perform a real-time measurement of optical aberrations is critical in many adaptive optics (AO) systems in which perfecting the image is realized by active mitigation of those aberrations [1]. The wide range of AO applications includes astronomy [2], free space optical communication [3], retinal imaging [4], OCT [5], and laser scanning microscopy [6,7]. One of the most common instruments for measuring aberrations is the Shack–Hartmann wavefront sensor (SHWS) [8], in which the local slopes of the wavefront are sampled using a microlens array (MLA), which generates a spot matrix on a camera. The local slopes are calculated based on the deviation of the spots from their initial position, resulting in a reconstructed wavefront. The simplicity of SHWS, which combines an off-the-shelf camera together with an MLA that can be manufactured in a mass-production fabrication process, makes it a preferred and common solution for wavefront sensing. Commercial versions of SHWS that can be found at relatively low prices serve as essential building blocks in many AO systems.

When working at wavelengths for which camera detectors are rare or very expensive, however, it becomes difficult to implement wavefront sensing using SHWS. At wavelengths in the near-infrared (NIR) region, one can find commercial solutions based on either phosphorus up-conversion [9] or an InGaAs camera [10]. Both solutions are more expensive and cover only a small portion of the NIR spectral region. For broader spectral response, it is possible to use a mercury cadmium telluride (MCT) camera [11] as a detector, but this is an expensive, custom solution, and it is not widely available.

Here, we introduce a two-photon (2P) SHWS that extends the working spectrum of any conventional SHWS from the visible range to the NIR. Our solution is based on two-photon absorption (TPA) in silicon, which allows detection of laser pulses even when the wavelength of the laser exceeds the linear spectral detection range of the material. In this way, by using a silicon-based SHWS, it is possible to measure the wavefront of a pulsed-laser beam up to 2200 nm with an off-the-shelf, cheap, commercial product.

TPA in semiconductors is a well-known phenomenon [12] in which two long-wavelength photons generate one photoelectron in the material. TPA in silicon photodiode (PD) is commonly used in autocorrelation for temporal measurement of short pulses [13] and plays an important role in silicon photonics applications such as fast optical modulators [14], high-speed optical logic gates [15], and telecom applications [16].

TPA was studied and demonstrated for laser pulses in silicon PD [17] and avalanche photodiode (APD) [18]. A silicon TPA cross section was characterized from 850 nm to 2200 nm [19]. Usually, high peak intensity is needed to generate a TPA signal. When using subpicosecond NIR laser pulses, the peak power becomes large enough to generate TPA even for small NA values. Such NIR pulsed lasers are common in fiber applications [20] and in multiphoton microscopy [21–24].

To demonstrate our solution, we used an off-the-shelf wavefront sensor (WFS150-7AR, Thorlabs) [Fig. 1(a)] that consists of a silicon CCD camera (1280 × 1024 pixels, pixel size of 4.65 μm) and a 39 × 31 MLA with an effective focal length of 5.2 mm and microlens pitch of 150 μm. The linear spectral response of the silicon-based camera is limited by the response of silicon as shown in Fig. 2. We used 3 wavelengths in the NIR—1550 nm, 1750 nm, and 2000 nm—in order to demonstrate the wavefront sensing performance in wavelengths outside the linear detection range of an InGaAs camera (which is limited to approximately 1700 nm).

We used a fiber laser (CAZADERO, Calmar lasers) that delivers 380 fs pulses at 1550 nm [Fig. 3(a)] with maximal pulse energy of 0.5 μJ at 4 MHz repetition rate. To generate 1750 nm and 2000 nm pulses, we coupled the light into a 1-m-long large mode area (LMA) fiber with ∼21 μm mode field diameter (LMA25, NKT). The high peak power of the coupled light generates a soliton pulse inside the LMA fiber, which shifts its central wavelength to a longer wavelength up to 2 μm

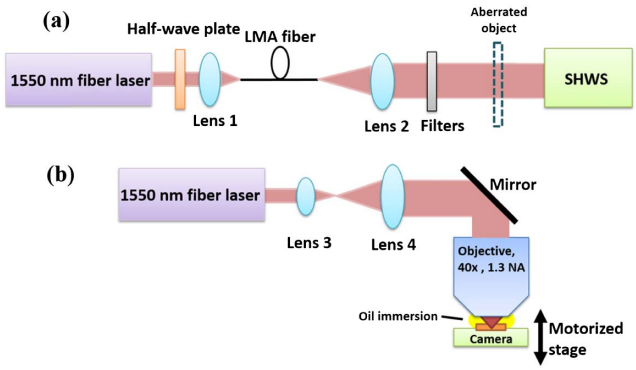

Fig. 1. Schematics of the experimental setups for (a) generating longer wavelengths for 2P SHWS demonstration. A fiber laser (CAZADERO, Calmar lasers) delivers 380 fs pulses with pulse energy up to 0.5 μJ at 1550 nm at 4 MHz repetition rate. LMA fiber: large-mode-area photonic crystal fiber (LMA25, NKT). Lens 1: $f = 45$ mm, Lens 2: $f = 50$ mm, (b) axial scanning of TPA response of a silicon CMOS camera sensor or a silicon CCD camera sensor. We used a high NA objective (Zeiss Plan-Neofluar 40 × /1.30) oil-immersion objective and overfilled its back aperture. Lens 3: $f = 50$ mm lens, Lens 4: $f = 150$ mm lens. Axial scan is performed with a motorized stage (MP-285, Sutter Instrument).

according to the input power [25,26] due to soliton self-frequency shift (SSFS). By using an input power of 300 mW and by spectral filtering of the LMA fiber output, we can get soliton pulses at 1750 nm with a pulse duration of 70 fs [Fig. 3(b)]. By increasing the input power to 1.2 W, the soliton was shifted to 2000 nm with a pulse duration of 100 fs [Fig. 3(c)]. For demonstration of the 2P SHWS, we first verify that the silicon-based detector response is indeed TPA at the longer wavelengths. We used the fiber laser source at 1550 nm and measured the output signal as a function of the input power. The results are shown in logarithmic scale in Fig. 4, where the slopes of the power dependence indicate the order of the nonlinear optical process. The measurements were performed for a silicon PD, a silicon CMOS camera, and a silicon CCD camera, all confirming two-photon response.

We used the illumination source operated at three different NIR wavelengths with several cylindrical lenses to measure wavefront aberrations. The results, shown in Figs. 5(a)–5(f), demonstrate that 2P SHWS can measure wavefront distortions introduced by the cylindrical lens at various orientations. In addition, Figs. 5(g)–5(i) show that the results match the

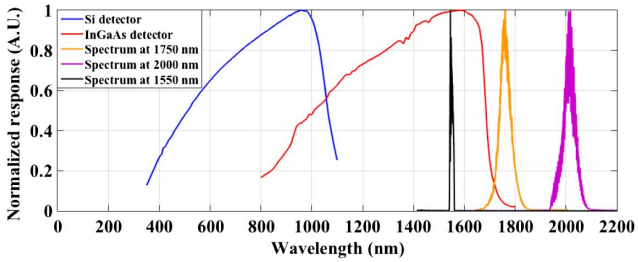

Fig. 2. Spectral response of the silicon-based detector (blue) and InGaAs detector (red), obtained from Thorlabs. Measured spectra of the fiber laser source at 1550 nm (black), the shifted soliton at 1750 nm (orange), and 2000 nm (purple).

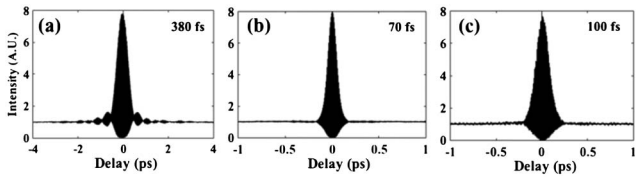

Fig. 3. Measured second-order interferometric autocorrelations of the laser pulses at (a) 1550 nm, (b) 1750 nm, and (c) 2000 nm. A deconvolution factor of 1.54 for sech^2-pulse was assumed to obtain the indicated pulse durations.

expected wavefront curvature, which corresponds to a cylindrical lens with a focal length of ∼200 mm.

Since the evaluation of the wavefront relies on geometrical calculation, the results are completely independent of the detection process. The same image processing and calibration used for linear detection can be used in 2P SHWS without any modification.

The main limitation of the 2P SHWS is detection sensitivity. In the following paragraphs, we will provide a detailed analysis and discuss the guidelines to optimize detection sensitivity of a 2P SHWS. We will evaluate the sensitivity by quantifying the lowest power needed for 2P SHWS and comparing it to that for a one-photon (1P) SHWS. The generation of photocurrents in 1P and 2P has completely different dependence on the SHWS geometry. For 1P SHWS, due to the strong 1P absorption of silicon at 400–1000 nm [27], photocurrent generation and detection occur within several microns of the detector surface. For 2P SHWS, the photocurrent depends critically on the axial spot size and detection depth. To maximize the 2P signal, the device layer for generation and detection of the 2P photocurrent should be larger than the axial spot size. We will show that in our current commercial SHWS, the depth of the silicon layer that generates and detects the TPA signal is much smaller than the axial spot size. We will then discuss the approaches to improve the detection sensitivity of the 2P SHWS by optimizing the design parameters.

To measure the lowest power level for the 2P SHWS, we reduced the incident power until the spot diagram of the SHWS was too noisy for wavefront reconstruction. We placed a 3-mm diameter aperture in front of the SHWS, an aperture that includes ∼300 microlenses. During all measurements, the SHWS was set to the maximal gain and exposure time (56 ms per frame) and averaged over 100 frames (total exposure time of 5.6 s). For 2P SHWS, we measured the minimum power using illumination sources at 1550 nm, 1750 nm, and 2000 nm. For 1P SHWS, we used a 635 nm CW laser (4/125-635-S-1, OZ Optics). The results are shown in Table 1.

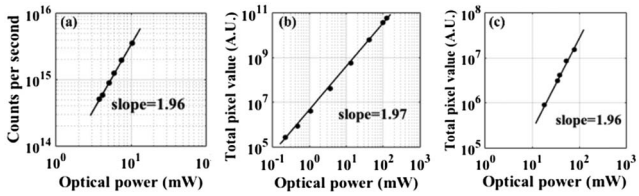

Fig. 4. Logarithmic plots measured with the 1550 nm laser pulses, showing the dependence of TPA signal on the incident power. (a) Silicon PD; (b) silicon CMOS camera; (c) silicon CCD camera.

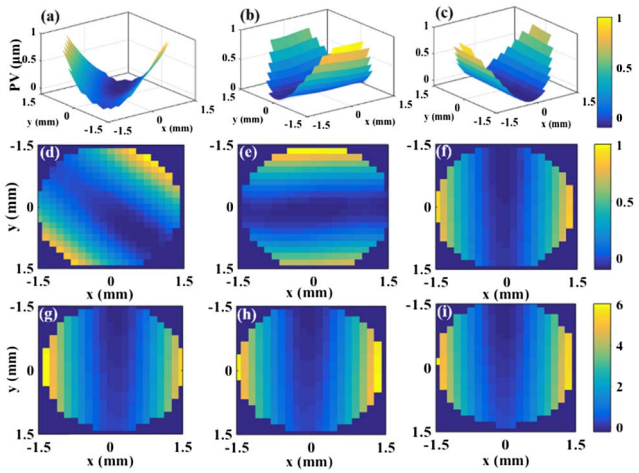

Fig. 5. Measured wavefronts of a 1000-mm-focal-length cylindrical lens at a wavelength of 2000 nm in different rotational orientations: (a), (d) 45°; (b), (e) 0°; (c), (f) 90°. PV: peak-to-valley value. (g)–(i) Measured wavefront of a 200-mm-focal-length cylindrical lens at different wavelengths: (g) 1550 nm, (h) 1750 nm, (i) 2000 nm.

The difference between the power limits of 1P SHWS and 2P SHWS is mainly caused by the vast difference in absorption by the linear and nonlinear processes. The variation of the measured TPA power limit at different wavelengths is due to the difference in the TPA coefficient and the pulse width [19].

To compare the minimum power results for 1P and 2P SHWS, we need to examine the signal dependence on the geometry in each case. We measured the layer thickness for the photocurrent generation and detection by using the 1550 nm laser source and scanning the detector axially through the focus of a high NA, oil-immersion objective [Fig. 1(b)] [28]. The TPA signals from the scan, shown in Fig. 6, provide the upper bound of the depth of the device layer for photocurrent generation and detection. We conducted the experiment for a silicon CMOS camera (DCC1545M, Thorlabs) and a silicon CCD camera (STC-MB152USB, Sentech), which has the same camera sensor model as in our wavefront sensor. The detectors were taken out of its mechanical package in order to allow the measurement with the oil-immersion objective. For silicon PD (SM1PD1A, Thorlabs), we used a similar setup with an air objective (Mitutoyo M Plan Apo 50 × , NA 0.42). The results, shown in Fig. 6, are ~400 μm for the silicon PD, ~30 μm for the silicon CMOS camera, and ~23 μm for the silicon CCD camera. All the values are much larger than the 1P absorption length at 635 nm (~3 μm) [27].

In the commercial SHWS, the NA of the MLA is small (for our MLA, the NA is 0.0144), resulting in an axial focal depth of a few millimeters. Due to the axial confinement of TPA, 2P photocurrent generation occurs mostly within the focal depth. However, because the focal depth of the low-NA MLA is several orders of magnitude larger than the measured thickness of the camera detection layer, this active layer thickness limits the TPA signal.

Table 1. Minimum Power for 1P and 2P SHWS Operation

Source	Visible	Fiber Laser	Wavelength Shifted Solitons	
Wavelength [nm]	635	1550	1750	2000
Pulse width [fs]	CW	380	70	100
Measured minimum power per microlens	0.2 pW	6.4 μW	2.3 μW	8.3 μW

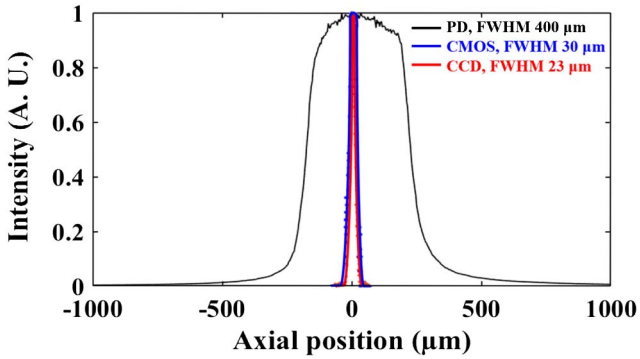

Fig. 6. Axial TPA response of a silicon photodiode (PD), a silicon CMOS camera sensor, and a silicon CCD camera sensor. The full width at half-maximum (FWHM) of the TPA response of the PD is 400 μm, 30 μm for the silicon CMOS camera sensor, and 23 μm for the silicon CCD camera sensor.

Using the measured sensitivities shown in Table 1, we can estimate the detection limit of 2P SHWS. We first calculate the number of photoelectrons using the measured power at 635 nm. The lateral spot radius is ~20 μm ($1/e^2$, under Gaussian approximation), which is much larger than the 4.65 μm pixel size of the camera. For simplicity, we compare only the number of photoelectrons on the central pixel. The number of photoelectrons $N^{(1)}(t)$ for the 1P process is

$$\langle N^{(1)}(t)\rangle = \eta \frac{2P^{(1)}(t)}{\pi\omega_1^2 h\nu_1}\Delta x\Delta y, \tag{1}$$

where η is the quantum efficiency, $P^{(1)}(t)$ is the power in Watts, ω_1 is the $1/e^2$ spot size radius of the beam, h is plank constant, ν_1 is the frequency of excitation light, and Δx, Δy are the pixel lateral dimensions (in our commercial WS $\Delta x = \Delta y = 4.65$ μm). For the TPA signal, we use the same formalism used for nonlinear fluorescence [29]. Since the focal depth is much larger than the measured thickness (Δz) of the active layer of the silicon-based camera, the TPA volume is determined by the pixel volume $\Delta x\Delta y\Delta z$, and the TPA signal $N^{(2)}(t)$ is, therefore, given by

$$\langle N^{(2)}(t)\rangle = \frac{1}{2}\frac{g_p^{(2)}}{f\tau}\eta\sigma_2 C\left(\frac{2P^{(2)}(t)/h\nu_2}{\pi\omega_2^2}\right)^2\Delta x\Delta y\Delta z, \tag{2}$$

where $g_p^{(2)}$ is the temporal coherence factor of the excitation laser source (0.59 for hyperbolic-secant-squared pulse), f is the laser repetition rate, τ is the laser pulse width, C is the concentration of the silicon atoms, σ_2 is the TPA cross section, $P^{(2)}(t)$ is the power in Watts, ν_2 is excitation light frequency, and ω_2 is the lateral spot size radius as was determined by the Gaussian approximation [30].

Assuming that the same number of photoelectrons is needed per microlens for generating a valid tilt at the detection threshold for 1P and 2P SHWS, we can calculate Δz independently by using Eqs. (1) and (2), together with the measured minimum power levels listed in Table 1 and the known nonlinear absorption coefficient of silicon [19,28,31]. We found that $\Delta z \cong 23$ μm. This result is in good agreement with the

measured value of ~23 μm for the silicon CCD camera sensor as shown in Fig. 6, taking into account the focal depth of the high NA lens (about 10 to 20 μm thick in silicon). The consistency of the 1P and 2P measurements provides a high degree of confidence that the minimum power measurements listed in Table 1 are indicative of the detection sensitivity of 2P SHWS using the commercially available SHWS.

Although in this work we used an off-the-shelf, commercial wavefront sensor, a few modifications can be done to improve the TPA signal, allowing wavefront measurement of longer pulse widths and at lower power levels. Using our measurement and analysis described above, we can estimate the detection limit for a well-optimized 2P SHWS.

Signal improvement can be achieved by reducing the focal depth so that the focal depth is smaller than the thickness of the active layer. This can be done either by increasing the NA of the microlens and reducing the lateral and axial spot size, or by fabricating a thicker active layer so that the axial spot size is fully confined within the active layer. The NA can be increased by using a microlens with shorter focal length and larger diameter. In order to maintain the angular sensitivity and dynamic range of the SHWS, a larger detector matrix with smaller pixel size may be needed, as long as the geometrical scaling of the system remains the same. Increasing the thickness of the layer should not affect the two-photon response, as shown in Figs. 4 and 6, where the TPA of a silicon PD with a thick detection layer is shown.

Once such a confinement is achieved, increasing the NA further will not enhance the TPA signal. Additional optimization can be obtained by changing the optical coating of the MLA and the detector material. An MLA with NA > 0.2 will be suitable for the current lateral pixel size, but will demand larger detection depth, where NA > 0.4 should be suitable for a regular camera. Using an optimally designed 2P SHWS, the focal volume is fully confined in the pixel detection volume, and the number of photoelectrons $N^{(2)}(t)$ from the TPA should be [29]

$$\langle N^{(2)}(t)\rangle = \frac{1}{2}\frac{g_p^{(2)}}{f\tau}\eta\sigma_2 C n_0 \frac{a_2\langle P^{(2)}(t)/h\nu_2\rangle^2}{8\pi\lambda_2}, \tag{3}$$

where n_0 is the refractive index of silicon, λ_2 is the wavelength of the excitation light, and a_2 is a volume integration factor dependent on the nonlinearity order ($a_2 = 64$ under paraxial approximation). By comparing Eqs. (2) and (3), we can calculate the minimum power (P_o) for TPA for an optimized 2P SHWS using the power levels (P) listed in Table 1:

$$P_o = P\sqrt{\frac{32\Delta x\Delta y\Delta z\lambda_2}{\pi\omega_2^4 n_0 a_2}}. \tag{4}$$

Using the same pulse characteristics at 1550 nm (380 fs pulse width, 4 MHz), the theoretical value for minimum power per microlens according to Eq. (4) should be ~16 nW, indicating a ~400-time improvement of the detection sensitivity compared to the measured result in Table 1. In this case, assuming a beam size of 3 mm with 300 microlenses, the minimal detected power for such a sub-picosecond pulse beam should be ~4.8 μW, which is equivalent to a pulse energy of ~1.2 pJ. The power level and pulse energy are compatible with most short pulse lasers for practical applications such as in telecom and biomedical imaging.

The wavefront sensing scheme described here is easy to implement without any modification of the SHWS. The ability to use a cheap, commercially available silicon-based camera as the detector of a 2P SHWS for NIR wavelengths can be valuable for many researchers. This concept is not limited only to NIR lasers, and can be applied to TPA beyond silicon, such as measuring up to 3.4 μm mid-infrared laser sources with TPA in InGaAs-based 2P SHWS. For wavelength up to 3 μm, it is also possible to use three-photon absorption as the detection mechanism [32]. However, this solution is suitable only for very strong, ultra-short pulses. We anticipate that many laser users in the NIR region would be able to apply our method to characterize their systems.

Funding. National Institutes of Health (NIH) (R21EY026391, U01NS090530).

†These authors contributed equally to this work.

REFERENCES

1. R. K. Tyson, *Principles of Adaptive Optics* (CRC Press, 2011), p. 111.
2. J. M. Beckers, Annu. Rev. Astron. Astrophys. **31**, 13 (1993).
3. T. Weyrauch and M. A. Vorontsov, *Free-Space Laser Communications* (Springer, 2004), p. 247.
4. J. Liang, B. Grimm, S. Goelz, and J. F. Bille, J. Opt. Soc. Am. A **11**, 1949 (1994).
5. B. Hermann, E. J. Fernández, A. Unterhuber, H. Sattmann, A. F. Fercher, W. Drexler, P. M. Prieto, and P. Artal, Opt. Lett. **29**, 2142 (2004).
6. M. A. A. Neil, R. Juškaitis, M. J. Booth, T. Wilson, T. Tanaka, and S. Kawata, J. Microsc. **200**, 105 (2000).
7. M. J. Booth, M. A. A. Neil, R. Juškaitis, and T. Wilson, Proc. Natl. Acad. Sci. USA **99**, 5788 (2002).
8. B. C. Platt and R. Shack, J. Refract. Surg. **17**, S573 (2001).
9. R. J. Meier, J. M. B. Simbürger, T. Soukka, and M. Schäferling, Anal. Chem. **86**, 5535 (2014).
10. T. Martin, R. Brubaker, P. Dixon, M. A. Gagliardi, and T. Sudol, *Defense and Security* (SPIE, 2005), p. 12.
11. P. Feautrier and J. C. Gach, Adaptive Optics for Extremely Large Telescopes 4–Conference Proceedings (2015), Vol. **1**.
12. J. H. Bechtel and W. L. Smith, Phys. Rev. B **13**, 3515 (1976).
13. C. Xu, J. M. Roth, W. H. Knox, and K. Bergman, Electron. Lett. **38**, 1 (2002).
14. C. Manolatou and M. Lipson, J. Lightwave Technol. **24**, 1433 (2006).
15. T. K. Liang, L. R. Nunes, M. Tsuchiya, K. S. Abedin, T. Miyazaki, D. V. Thourhout, W. Bogaerts, P. Dumon, R. Baets, and H. K. Tsang, Opt. Commun. **265**, 171 (2006).
16. T. K. Liang and H. K. Tsang, Appl. Phys. Lett. **84**, 2745 (2004).
17. L. P. Barry, P. G. Bollond, J. M. Dudley, J. D. Harvey, and R. Leonhardt, Electron. Lett. **32**, 1922 (1996).
18. K. Kikuchi, Electron. Lett. **34**, 123 (1998).
19. A. D. Bristow, N. Rotenberg, and H. M. Van Driel, Appl. Phys. Lett. **90**, 191104 (2007).
20. K. Tamura, E. P. Ippen, H. A. Haus, and L. E. Nelson, Opt. Lett. **18**, 1080 (1993).
21. W. R. Zipfel, R. M. Williams, and W. W. Webb, Nat. Biotechnol. **21**, 1369 (2003).
22. F. Helmchen and W. Denk, Nat. Methods **2**, 932 (2005).
23. D. Kobat, N. G. Horton, and C. Xu, J. Biomed. Opt. **16**, 106014 (2011).
24. N. G. Horton, K. Wang, D. Kobat, C. G. Clark, F. W. Wise, C. B. Schaffer, and C. Xu, Nat. Photonics **7**, 205 (2013).
25. J. P. Gordon, Opt. Lett. **11**, 662 (1986).
26. J. H. Lee, J. V. Howe, C. Xu, and X. Liu, IEEE J. Sel. Top. Quantum Electron. **14**, 713 (2008).
27. M. A. Green, Sol. Energy Mater. Sol. Cells **92**, 1305 (2008).
28. C. Xu and W. Denk, J. Appl. Phys. **86**, 2226 (1999).
29. C. Xu and W. W. Webb, *Topics in Fluorescence Spectroscopy* (Springer, 2002), p. 471.
30. B. Zhang, J. Zerubia, and J. Olivo-Marin, Appl. Opt. **46**, 1819 (2007).
31. M. Bass, *Handbook of Optics*, 2nd ed. (McGraw-Hill, 1994), Vol. I, p. 32.
32. Y. Wei, S. Howard, A. Straub, Z. Wang, J. Cheng, S. Gao, and C. Xu, Opt. Lett. **36**, 2372 (2011).